

UCSF

UC San Francisco Previously Published Works

Title

Magnetic Resonance Imaging of the Lumbar Spine: Recommendations for Acquisition and Image Evaluation from the BACPAC Spine Imaging Working Group.

Permalink

<https://escholarship.org/uc/item/8qd6b084>

Journal

Pain Medicine, 24(Suppl 1)

Authors

Sollmann, Nico

Fields, Aaron

ONeill, Conor

et al.

Publication Date

2023-08-04

DOI

10.1093/pm/pnac130

Copyright Information

This work is made available under the terms of a Creative Commons Attribution License, available at <https://creativecommons.org/licenses/by/4.0/>

Peer reviewed

Magnetic Resonance Imaging of the Lumbar Spine: Recommendations for Acquisition and Image Evaluation from the BACPAC Spine Imaging Working Group

Nico Sollmann, MD, PhD,^{1,2,3,4} Aaron J. Fields, PhD,⁵ Conor O'Neill, MD,⁵ Lorenzo Nardo, MD, PhD,⁶ Sharmila Majumdar, PhD,^{1,7} Cynthia T. Chin, MD,¹ Duygu Tosun, PhD,¹ Misung Han, PhD,¹ An T. Vu, PhD,^{1,8} Eugene Ozhinsky, PhD,^{1,8} Lubdha M. Shah, MD,⁹ Richard E. Harris, PhD,¹⁰ Remy Lobo, MD,¹¹ William Anderst, PhD,¹² Richard Herzog, MD,¹³ Matthew A. Psioda, PhD,¹⁴ Christopher J. Standaert, MD,¹⁵ River T. Price,¹⁴ Jeffrey C. Lotz, PhD,⁵ Thomas M. Link, MD,¹ Roland Krug, PhD¹

¹Department of Radiology and Biomedical Imaging, University of California San Francisco, San Francisco, California, USA

²Department of Diagnostic and Interventional Radiology, University Hospital Ulm, Ulm, Germany

³Department of Diagnostic and Interventional Neuroradiology, School of Medicine, Klinikum rechts der Isar, Technical University of Munich, Munich, Germany

⁴TUM-Neuroimaging Center, Klinikum rechts der Isar, Technical University of Munich, Munich, Germany

⁵Department of Orthopaedic Surgery, University of California San Francisco, San Francisco, California, USA

⁶Department of Radiology, University of California, Davis, Sacramento, California, USA

⁷Center for Digital Health Innovation, University of California San Francisco, San Francisco, California, USA

⁸VA Advanced Imaging Research Center, San Francisco VA Health Care System, San Francisco, California, USA

⁹Department of Radiology, University of Utah, Salt Lake City, Utah, USA

¹⁰Department of Anesthesiology, University of Michigan, Ann Arbor, Michigan, USA

¹¹Department of Radiology, University of Michigan, Ann Arbor, Michigan, USA

¹²Department of Orthopaedic Surgery, University of Pittsburgh, Pittsburgh, Pennsylvania, USA

¹³Department of Radiology and Imaging, Hospital for Special Surgery, New York, New York, USA

¹⁴Department of Biostatistics, Gillings School of Global Public Health, University of North Carolina at Chapel Hill, Chapel Hill, North Carolina, USA

¹⁵Department of Physical Medicine and Rehabilitation, University of Pittsburgh School of Medicine, Pittsburgh, Pennsylvania, USA

*Correspondence to: Nico Sollmann, MD, PhD, Department of Radiology and Biomedical Imaging, University of California San Francisco, 85 Berry St, Lobby 6, San Francisco, CA 94107, USA. Tel: +1 415 353 4500; Fax: +1 415 353 4522; E-mail: nico.sollmann@tum.de.

Abstract

Management of patients suffering from low back pain (LBP) is challenging and requires development of diagnostic techniques to identify specific patient subgroups and phenotypes in order to customize treatment and predict clinical outcome. The Back Pain Consortium (BACPAC) Research Program Spine Imaging Working Group has developed standard operating procedures (SOPs) for spinal imaging protocols to be used in all BACPAC studies. These SOPs include procedures to conduct spinal imaging assessments with guidelines for standardizing the collection, reading/grading (using structured reporting with semi-quantitative evaluation using ordinal rating scales), and storage of images. This article presents the approach to image acquisition and evaluation recommended by the BACPAC Spine Imaging Working Group. While the approach is specific to BACPAC studies, it is general enough to be applied at other centers performing magnetic resonance imaging (MRI) acquisitions in patients with LBP. The herein presented SOPs are meant to improve understanding of pain mechanisms and facilitate patient phenotyping by codifying MRI-based methods that provide standardized, non-invasive assessments of spinal pathologies. Finally, these recommended procedures may facilitate the integration of better harmonized MRI data of the lumbar spine across studies and sites within and outside of BACPAC studies.

Keywords: Magnetic Resonance Imaging; Intervertebral Disc Degeneration; Low Back Pain; Paraspinal Musculature; Vertebral Endplate

Introduction

Magnetic resonance imaging (MRI) is the imaging modality often used to depict spinal structural abnormalities that may cause low back pain (LBP). With its high soft tissue contrast, MRI allows assessment of multiple structures including intervertebral discs, nerve roots, contents of the central spinal canal, ligaments and facet joints [1–5]. While MRI is superb at identifying tissue-specific pathology along the spine, the clinical relevance of these findings is often uncertain. Thus, diagnostic MRI for LBP is only recommended in certain

patients. The American College of Physicians' guidelines for diagnostic imaging suggest immediate imaging when there are major risks (such as suspicion of cancer, spinal infection, cauda equina syndrome, or presence of severe neurological deficits), but advise deferral of imaging pending a trial of treatment in cases where there are weaker risk factors [6, 7]. Notably, only in a minority of patients can LBP be attributed to a specific pathology (e.g., vertebral fracture or disc herniation with nerve compression), while the great majority of patients are assigned a diagnosis of non-specific LBP (i.e.,

pain for which the distinct patho-anatomical basis cannot be determined) [7, 8].

Some lumbar MRI findings that are common in patients with LBP are also common in asymptomatic subjects, which makes it difficult to define a causal relationship in individual patients and has led to questions about the diagnostic value of such findings [9–11]. However, some lumbar MRI findings are more prevalent in patients with LBP than in asymptomatic subjects [10–12]. Those include bone marrow (BM) lesions located at the vertebral endplates, disc bulges and herniation, and spondylolysis [10–12]. Such lumbar MRI findings could potentially function as biomarkers that can distinguish patients whose pain is due to a primary nociceptive process in the spine from patients with central modulating mechanisms that can be influenced by a number of psychosocial factors as well as central sensitization (i.e., increased responsiveness of nociceptors to either normal or sub-threshold afferent input, resulting in amplified pain) [13–16].

A major focus of the Back Pain Consortium (BACPAC) Research Program is to advance knowledge of the etiology and treatment of chronic LBP by developing a better understanding of the mechanisms contributing to chronic LBP and by identifying specific therapies that are most effective in identifiable subgroups of patients. The BACPAC Spine Imaging Working Group has developed standard operating procedures (SOPs) for lumbar spine imaging exams to be used in all BACPAC studies. These SOPs include procedures to conduct imaging assessments with guidelines for standardizing the collection, reading/grading, and storage of images across studies and sites within and outside of BACPAC. Our aim was to harmonize imaging protocols and implement a comprehensive evaluation scheme for identifying potential imaging biomarkers of LBP.

Imaging Protocol

Setup and Sequence Planning

Patients eligible for BACPAC studies will undergo an MRI examination (acquisition duration <60 min, depending on the distinct pulse sequence protocol) that is performed in a supine position using a spine coil or a table-embedded coil array. Following an initial phase of sequence optimization at each BACPAC site (including testing and determination of flip angles, fat suppression [FS] parameters, field of view [FOV] sizes, and subject/coil configurations for an optimized signal-to-noise ratio), MRI acquisition with a standardized pulse sequence protocol is performed. The recommendations of the BACPAC Spine Imaging Working Group regarding the distinct pulse sequence protocols refer to non-contrast MRI using a 3-Tesla or 1.5-Tesla MRI scanner. Furthermore, recommended is the use of the available clinical protocol for lumbar spine imaging as a starting point and make adjustments, if necessary, as described below.

Sequences will be manually planned (i.e., positioning and angulation of the FOV) using an initially acquired survey scan. At least the entire lumbosacral spine in cranio-caudal direction as well as the complete diameter of the vertebrae, facet joints (FJs), neuroforamina, and paraspinal musculature in transverse direction (and for predefined sequences also the sacroiliac joints [SIJs]) will be covered. When magnetic resonance neurography (MRN) of the lumbosacral plexus is additionally acquired, the anterior body coil (or torso coil) array

should be used in addition to the spine coil or table-embedded coil array, and the FOV should cover the area from L1/L2 through the ischial tuberosities.

Imaging Sequences

Regarding imaging with T1- and T2-weighted sequences, the BACPAC Spine Imaging Working Group recommends a minimal pulse sequence protocol that will be acquired in each patient, supplemented by additional sequences based on technical infrastructure at the acquisition site:

- a) Minimal recommended sequence protocol:
 - Sagittal T2-weighted fast spin-echo (FSE) sequence with FS: sagittal T2 FS
 - Sagittal T1-weighted FSE sequence without FS: sagittal T1
 - Axial T2-weighted FSE sequence without FS: axial T2
- b) Additional recommended sequences (if feasible):
 - Sagittal T2-weighted FSE sequence without FS: sagittal T2
 - Sagittal T1-weighted FSE sequence without FS (covering the SIJ): sagittal T1
 - Coronal T1-weighted FSE sequence without FS (covering the SIJ): coronal T1
 - Axial T1-weighted FSE sequence without FS: axial T1
 - MRN lumbosacral plexus: three-dimensional (3D) T2-weighted FSE sequence with FS: axial MRN

The specific parameters for these T1- and T2-weighted FSE sequences used for the MRI machine (GE 3T Discovery MR750; GE Healthcare, Waukesha, WI, USA) and coil (8-channel phased-array spine coil; GE Healthcare, Waukesha, WI, USA) at one site of image acquisitions are shown in [Table 1](#). Due to variations of pulse sequence implementations and hardware specifics between different MRI machines or vendors, ranges for pulse sequence protocols are proposed and shown in [Table 2](#).

Of note, the preference for specific echo times (TEs) of T2-weighted FSE sequences can also vary depending on whether structures within vertebral bodies and intervertebral discs are more important (typical TE around 60 ms), or depictions of spinal cord and nerves are more important (longer TEs, 80 ms or higher). As an additional recommended sequence, dedicated 3D MRN can be acquired in selected cases to delineate the peripheral nerves of the lumbosacral plexus for diagnosis and characterization of neuropathy (e.g., due to compressive effects in relation to a herniated disc) [17–22].

Evaluation of Imaging Data

Based on the MRI data acquired, we propose qualitative/semi-quantitative image evaluation (e.g., using ordinal rating scales) using structured reporting with a predefined scoring system that incorporates the different structures and related grading of pathology as captured by the FOV of the T1- and T2-weighted sequences (Modic-type endplate changes, endplate defects, intervertebral disc changes, FJ and SIJ changes, and stenosis).

Modic Changes

Modic-type endplate changes summarize three categories based on specific signal characteristics of vertebral BM adjacent to the endplates in MRI [23]. Most commonly, type 1

Table 1. Pulse sequence parameters for conventional T1- and T2-weighted sequences (standardized protocol)

| Sequence (Lumbosacral) | SAG T2 FS (Lumbar) | SAG T2 (Lumbar) | SAG T1 (Lumbar) | AX T2 (Lumbar) | AX T1 (Lumbar) | SAG T1 (with SIJ) | COR T1 (with SIJ) | AX MRN |
|---------------------------------|--------------------|--------------------|--------------------|--------------------|--------------------|--------------------|--------------------|--------------------------------|
| Patient Position | Head first, supine | Feet first, supine |
| Plane | SAG | SAG | SAG | AX | AX | SAG | COR | AX |
| Flip Angle [°] | 120 | 120 | 110 | 120 | 110 | 115 | 115 | Variable Refocusing Flip Angle |
| TE [ms] | 60 | 60 | 14.1 | 60 | 14.1 | 14.1 | 14.1 | 100 |
| TR [ms] | 4,551 | 5,035 | 869 | 8,414 | 594 | 720 | 595 | 2,500 |
| Echo Train Length | 16 | 18 | 6 | 16 | 6 | 6 | 6 | 100 |
| Receiver Bandwidth [kHz/0.5FOV] | 50 | 50 | 50 | 50 | 50 | 50 | 50 | 62.5 |
| FOV [cm] | 26 | 26 | 26 | 18 | 18 | 30 | 30 | 36x29 |
| Slice Thickness [mm] | 3.0 | 3.0 | 3.0 | 4.0 | 4.0 | 8.0 | 4.0 | 1.2 |
| Slice Spacing [mm] | 3.0 | 3.0 | 3.0 | 5.0 | 5.0 | 10 | 5.0 | N/A |
| Frequency Matrix | 384 | 384 | 384 | 288 | 288 | 320 | 384 | 300 |
| Phase Matrix | 224 | 224 | 224 | 192 | 192 | 160 | 224 | 240 |
| Frequency Direction | A/P | A/P | A/P | R/L | R/L | A/P | R/L | R/L |
| NEX averages | 3.0 | 3.0 | 2.0 | 2.0 | 2.0 | 2.0 | 2.0 | 1.0 |
| Fat suppression | On | Off | Off | Off | Off | Off | Off | On |
| Acceleration | Off | On |
| Number of Slices | 24 | 24 | 24 | 42 | 42 | 36 | 20 | 120 |
| Scan Time [min: sec] | 3:16 | 3:16 | 3:34 | 3:31 | 3:47 | 2:06 | 1:42 | 8:30 |

This table shows the sequence parameters for the conventional T1-/T2-weighted sequences for the main site’s magnetic resonance imaging (MRI) system (GE 3 T Discovery MR750; GE Healthcare, Waukesha, WI, USA). For MRN, acceleration is achieved with $2 \times 1.5 \times 1.4$ (ky phase-encode direction \times kz phase-encode direction \times compressed sensing factor).

AX = axial; SAG = sagittal; COR = coronal; FS = fat suppression; TE = echo time; TR = repetition time; FOV = field of view; R/L = right/left; A/P = anterior/posterior; NEX = number of excitations (averages); SIJ = sacroiliac joint.

Table 2. Pulse sequence parameters for conventional T1- and T2-weighted sequences (recommended ranges)

| Sequence (Lumbosacral) | SAG T2 FS (Lumbar) | SAG T2 (Lumbar) | SAG T1 (Lumbar) | AX T2 (Lumbar) | AX T1 (Lumbar) | SAG T1 (with SIJ) | COR T1 (with SIJ) | AX MRN |
|---------------------------------|--------------------|--------------------|--------------------|--------------------|--------------------|--------------------|--------------------|---------------------|
| Patient Position | Head first, supine | Feet first, supine |
| Plane | SAG | SAG | SAG | AX | AX | SAG | COR | AX |
| Flip Angle [°] | 105–180 | 105–180 | 105–180 | 105–180 | 105–180 | 105–180 | 105–180 | Variable Flip Angle |
| TE [ms] | 40–80 | 40–80 | 8–20 | 40–80 | 8–20 | 8–20 | 8–20 | 80–120 |
| TR [ms] | $\geq 2,000$ | $\geq 2,000$ | 500–900 | $\geq 2,000$ | 500–900 | 500–900 | 500–900 | 1,500–2,500 |
| Echo Train Length | 15–24 | 15–24 | 3–8 | 15–24 | 3–8 | 3–8 | 3–8 | 60–120 |
| Receiver Bandwidth [kHz/0.5FOV] | 31–62 | 31–62 | 31–62 | 31–62 | 31–62 | 31–62 | 31–62 | 31–62.5 |
| FOV [cm] | 25–28 | 25–28 | 25–28 | 14–22 | 14–22 | 30–32 | 26–32 | 36–38 |
| Slice Thickness [mm] | ≤ 4.0 | ≤ 8.0 | ≤ 4.0 | ≤ 1.5 |
| Slice Spacing [mm] | ≤ 4 | ≤ 4 | ≤ 4 | ≤ 5 | ≤ 5 | ≤ 10 | ≤ 5 | N/A |
| Frequency Matrix | 320–512 | 320–512 | 320–512 | 256–512 | 256–512 | 320–512 | 256–512 | 256–380 |
| Phase Matrix | 192–320 | 192–320 | 192–320 | 192–320 | 192–320 | 160–320 | 192–320 | 200–304 |
| Frequency Direction | A/P | A/P | A/P | R/L | R/L | A/P | R/L | R/L |
| NEX averages | 1–4 | 1–4 | 1–4 | 1–4 | 1–4 | 1–4 | 1–4 | 1 |
| Fat suppression | On | Off | Off | Off | Off | Off | Off | On |
| Number of Slices | ≥ 12 | ≥ 12 | ≥ 12 | ≥ 30 | ≥ 30 | ≥ 30 | ≥ 12 | N/A |
| Scan Time [min] | ≤ 5 min | ≤ 4 min | ≤ 3 min | ≤ 10 min |

Due to variations in magnetic resonance imaging (MRI) machines and vendors between imaging sites, ranges for pulse sequence protocols are proposed for conventional T1-/T2-weighted sequences.

AX = axial; SAG = sagittal; COR = coronal; FS = fat suppression; TE = echo time; TR = repetition time; FOV = field of view; R/L = right/left; A/P = anterior/posterior; NEX = number of excitations (averages); SIJ = sacroiliac joint.

Table 3. Modic-type endplate changes

| | 0 | 1 | 2 | 3 | 4 | Sequences |
|---|--------|---|--|--|--|-------------------------------|
| Modic Changes | absent | present | | | | |
| Modic Type | | T1: hypointense T2: hyperintense T2 FS: hyperintense | T1: hyperintense T2: hyperintense T2 FS: iso-/hypo- intense | T1: hypointense T2: hypointense T2 FS: hypointense | | SAG T2 SAG T1 SAG T2 FS |
| Vertebral Body Height | | Localized at endplate only | Less than 25% of vertebral body height | 25 to 50% of verte- bral body height | More than 50% of vertebral body height | SAG T2 SAG T1 SAG T2 FS |
| Affected Endplate Area (largest diameter in a single section) | | Less than 25% of endplate area | 25 to 50% of end- plate area | More than 50% of endplate area | | SAG T2 SAG T1 SAG T2 FS |

This table provides the scoring scheme for Modic changes and the sequences used for evaluation of different categories. In case that Modic changes are detected, the type (Modic type I—III) as well as the spatial characteristics of changes with respect to vertebral body height and vertebral endplate area should be graded.

changes are considered an inflammatory, fibrovascular stage and may indicate an ongoing active degenerative process (e.g., disruption and fissuring of endplates and formation of granulation tissue) [23, 24]. Type 2 changes are related to fatty degenerative remodeling processes, with replacement of red by yellow BM within the vertebrae [23, 24]. Furthermore, type 3 changes reflect the sclerotic stage [23, 24]. Related to their suggested pathophysiological entity, the three different types of Modic-type endplate changes differ in their appearances using the combination of sagittal T1- and T2-weighted sequences, with Modic changes type 1 typically showing hypointense signal on T1- and hyperintense signal on T2-weighted images, Modic changes type 2 showing hyperintense signal on T1- and hyper- or iso-intense signal on T2-weighted images without FS (typically relatively hypointense on T2-weighted images with FS), and Modic changes type 3 showing hypointense signal on T1- and T2-weighted images [23, 25, 26]. However, mixed types can be observed frequently for one lumbar segment (e.g., presence of signal characteristics indicative of Modic changes type 1 and type 2), and categorization may be done by reporting the dominant type.

Regarding reliability of assessments of Modic-type endplate changes on lumbar MRI, literature reports on varying but substantial to excellent intra-rater agreement ($\kappa > 0.70$) and inter-rater agreement ($\kappa > 0.78$) [27, 28]. Furthermore, the diagnostic performance of the Modic classification for discography-concordant pain yielded a specificity of at least 95% [29–33]. However, corresponding sensitivity was reported to be rather low and variable, with values ranging between 14% and 48% [29–33]. In addition to classifications into the three types of Modic-type endplate changes, the extent of changes in relation to vertebral body height and diameter is determined (Table 3). Example cases for Modic-type endplate changes are shown in Figure 1.

Endplate Defects

Structural changes at the vertebral endplates are scored according to their appearance into degenerative changes (e.g., erosive intervertebral osteochondrosis), Scheuermann variant, and osteoporotic fractures. Erosive intervertebral osteochondrosis entails widespread erosions of the vertebral body endplates with disc degeneration, commonly leading to findings of vacuum phenomenon within the intervertebral disc, hypointensity within the intervertebral disc on T2-weighted images, band-like subchondral edema, and fat accumulation or sclerosis for affected vertebral bodies [34]. Scheuermann

variant is a developmental disorder with a hereditary predisposition component, with characteristic features of thoracic spine kyphosis $>40^\circ$ or thoraco-lumbar spine kyphosis $>30^\circ$ and vertebral wedge configuration of at least 5° at each level, involving at least three adjacent vertebral bodies according to the Sorensen criteria [35, 36]. A differential diagnosis is represented by changes of vertebral body configuration due to osteoporotic fractures, which can also appear as wedging of one or more vertebral bodies [37, 38]. However, the entity is different, with osteoporosis being characterized by low bone mineral density in combination with micro-architectural deterioration of bone tissue, thus increasing the risk for fragility fractures [39–44]. To provide further insights into the distinct appearance of endplate defects, they are further categorized according to shape as well as size and depth for a representative section (Table 4). Example cases for endplate defects are illustrated by Figure 2.

Intervertebral Disc Changes

Lumbar disc degeneration is graded according to the widely used Pfirrmann classification, which defines five grades in total according to the intervertebral disc height as well as signal characteristics shown on T2-weighted sequences [45]. Specifically, it spans from grade I for a homogeneous disc with normal height and bright hyperintense white signal intensity to grade V for an inhomogeneous disc with collapsed disc space and a hypointense black signal intensity [45]. The Pfirrmann classification for degenerative disc disease has been reported to show substantial to excellent inter-rater ($\kappa > 0.65$) and intra-rater ($\kappa > 0.73$) reliability [45–48]. This grading is supplemented by information on potential contact between disc material and nerve roots, or deviation or compression of nerve roots due to disc degeneration (Table 5) [49].

Furthermore, location and morphology of disc herniation is classified according to shape characteristics, including bulge, protrusion, and extrusion [50, 51]. Specifically, bulge is defined as annular tissue that projects beyond the margins of the adjacent vertebral bodies, affecting more than 90° of circumference [50, 51]. A disc protrusion is a focal herniation of disc material beyond the margins of the adjacent vertebral bodies (over less than 90° of circumference and with a base that is wider than the dome) [50, 51]. In addition, a disc extrusion is a focal herniation of disc nuclear material through an annular defect (remaining in continuity with the disc and with a base narrower than the dome) [50, 51].



Figure 1. Modic-type endplate changes. Examples of Modic-type endplate changes, which can be identified according to characteristic signal alterations in T1- and T2-weighted images. Modic changes type 1 are typically hypointense on T1- and hyperintense on T2-weighted images (a; arrowheads), and Modic changes type 2 are hyperintense on T1- and hyper- or iso-intense on T2-weighted images without fat suppression (b; arrowheads). Modic type 3 changes are primarily characterized by sclerotic changes (not shown).

Table 4. Endplate defects

| | 0 | 1 | 2 | 3 | 4 | Sequences |
|--|--------|--|---|---|-------|------------------|
| Endplate Defect Type | Absent | Present Degenerative (e.g., erosive intervertebral osteochondrosis) | Scheuermann variant (Schmorl’s nodes); wedge-shaped deformity and increased sagittal diameter | Osteoporotic (normal sagittal diameter) | Other | SAG T1 SAG T2 |
| Shape | | Irregular, diffuse | Schmorl’s node, subchondral cyst | Sharp, angular, focal | Other | SAG T1 SAG T2 |
| Size (largest diameter in a single section) | | Less than 1/3 of endplate area | Between 1/3 and 2/3 of endplate area | More than 2/3 of endplate area | | SAG T1 SAG T2 |
| Depth (largest diameter in a single section) | | Less than 25% of vertebral body height | 25 to 50% of vertebral body height | More than 50% of vertebral body height | | SAG T1 SAG T2 |

This table outlines the scoring scheme for vertebral endplate defects and the sequences used for evaluation of single categories. In case that vertebral endplate defects are detected, the type as well as the spatial characteristics of changes with respect to vertebral body height and vertebral endplate area should be graded, as well as their shapes.

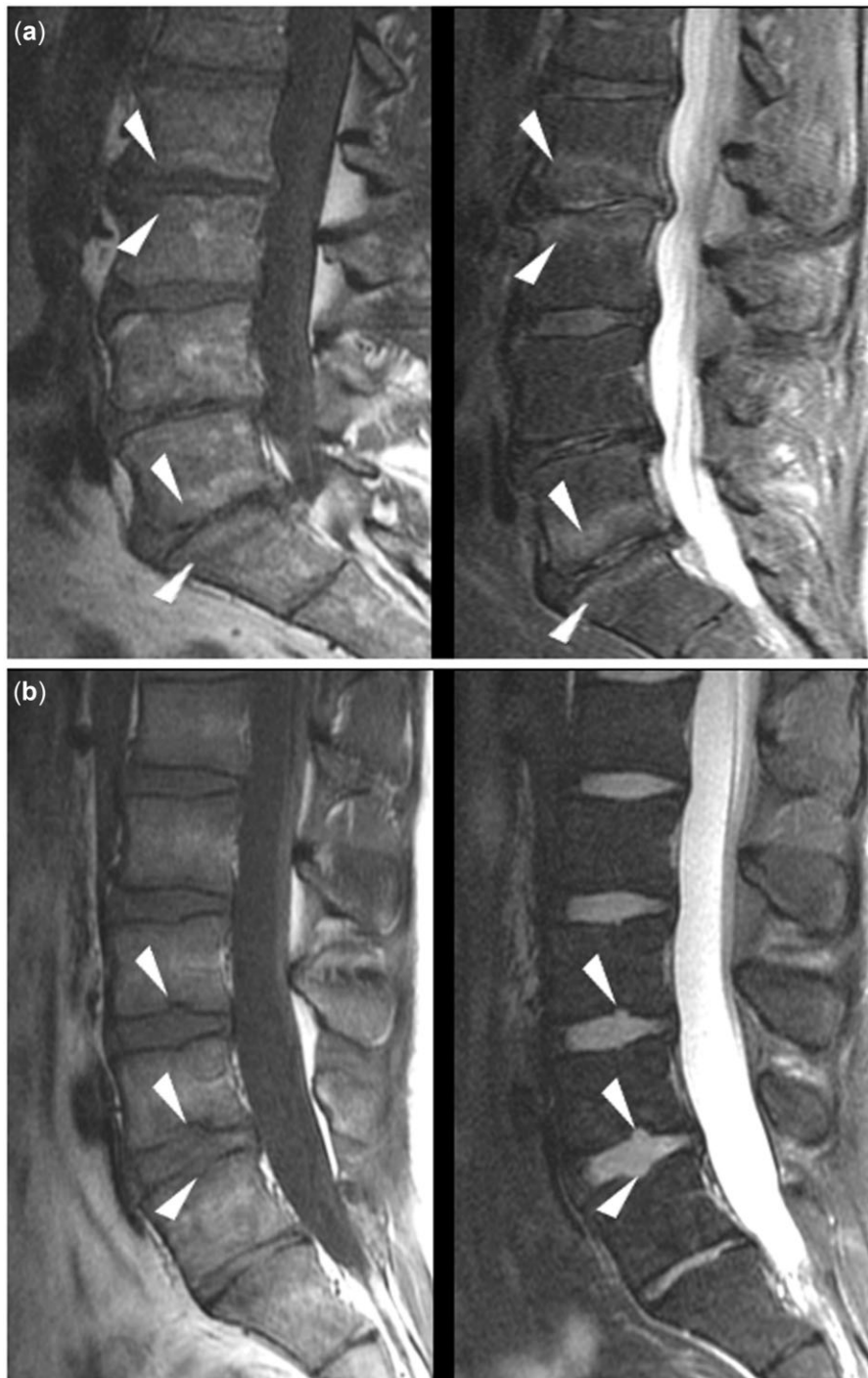


Figure 2. Endplate defects. Examples of endplate defects with degenerative appearance (erosive osteochondrosis) on T1- and T2-weighted sequences (a; arrowheads) and focal Schmorl's nodes on T1- and T2-weighted sequences (b; arrowheads).

Additionally, the absence or presence of an annular fissure and its location is taken into consideration, which is commonly characterized by a zone of high signal on T2-weighted images at the lateral edges of the annulus (Table 5) [50, 51]. Example cases for degenerative disc disease are provided by Figures 3 and 4.

Facet and Sacroiliac Joint Changes

Arthropathies of the FJ or SIJ are typically characterized by joint space reductions, hypertrophy of articular processes, and formation of osteophytes. For the FJs, grading into four

groups according to these characteristics is made with respect to the grading approaches by Fujiwara and Pathria and their coworkers (Table 6) [52, 53]. For grading of FJ arthropathy using MRI, a rather weak inter-rater reliability ($\kappa > 0.40$) has been reported, although this grading has been widely used [46, 54]. Example cases for FJ arthropathy grading are shown in Figure 5.

For the SIJ, edematous or fatty changes are evaluated, together with presence or absence of insufficiency fractures or alterations suggestive for osteitis condensans ilii [55–57]. Furthermore, the presence and degrees of lumbosacral

Table 5. Intervertebral disc changes

| | 0 | 1 | 2 | 3 | 4 | 5 | Sequences |
|-------------------------------|---------------------------|---|---|--|--|---|---------------------------|
| Degenerative Disc Disease | | Homogeneous, hyperintense, normal height | Inhomogeneous, hyperintense, normal height, clear distinction annulus vs. nucleus | Inhomogeneous, gray, normal height, no clear distinction between annulus vs. nucleus | Inhomogeneous, gray to black, normal height to moderate loss, no distinction between annulus vs. nucleus | Inhomogeneous, black, > 50% height loss | SAG T2 |
| Disc Height | Less than 10% loss (mild) | 10%–50% loss (moderate) | >50% loss (severe) | | | | SAG T2 |
| Disc Herniation | Normal | Bulge | Protrusion | Extrusion | | | SAG T2 FS AX T2 |
| Protrusion/Extrusion Location | Central | Subarticular zone | Foraminal | Extraforaminal | | | SAG T2 |
| Protrusion/Extrusion Side | Left | Right | | | | | SAG T2 |
| Annular Fissure | Absent | Present | | | | | SAG T2 |
| Annular Fissure location | Central/posterior | Left/subarticular | Right/subarticular | | | | SAG T2 |
| Nerve Root Involvement | No nerve root contact | Nerve root—left contact without deviation | Nerve root—left deviation and compression | Nerve root—right contact without deviation | Nerve root—right deviation and compression | Bilateral | SAG T1 SAG T2 AX T2 |

This table shows the scoring scheme for intervertebral disc changes and the sequences used for evaluation of respective categories. In case that degenerative disc disease is detected, its characteristics including signal, height, herniation specifics, and nerve root involvement should be graded, together with screening for an annular fissure.

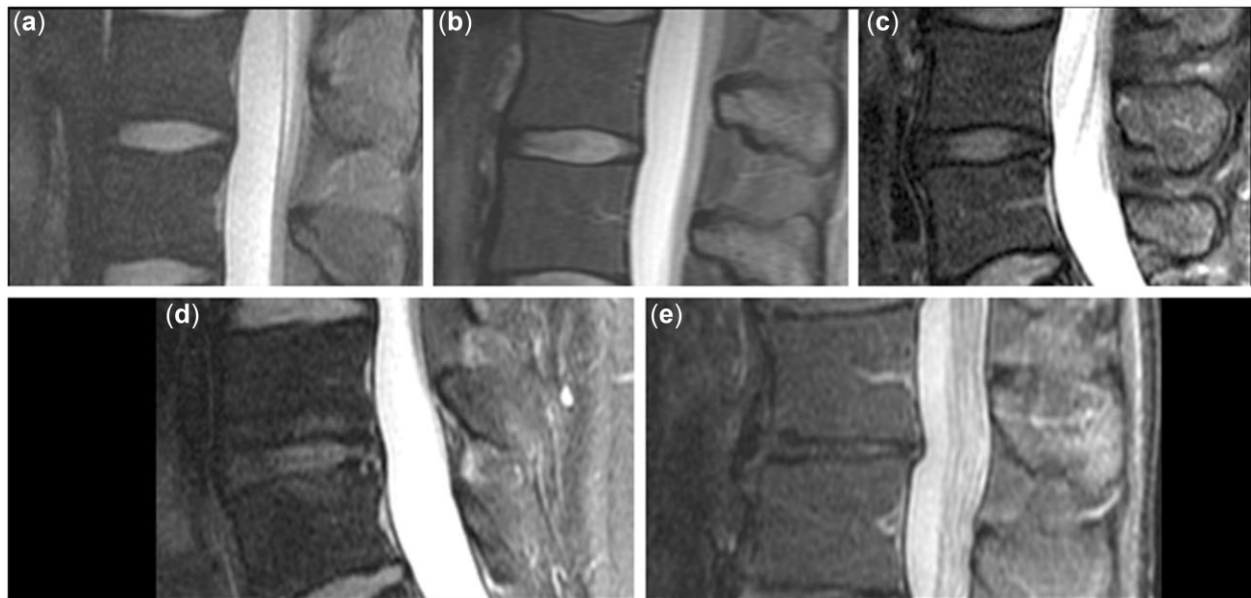


Figure 3. Degenerative disc disease. Examples for grading of intervertebral discs: homogeneous, hyperintense, normal height of disc (a; Pfirrmann grade I); inhomogeneous, hyperintense, normal height, clear distinction annulus versus nucleus (b; Pfirrmann grade II); inhomogeneous, gray, normal height, no clear distinction between annulus versus nucleus (c; Pfirrmann grade III); inhomogeneous, gray to black, normal height to moderate loss, no distinction between annulus versus nucleus (d; Pfirrmann grade IV); and inhomogeneous, black, > 50% height loss (e; Pfirrmann grade V).

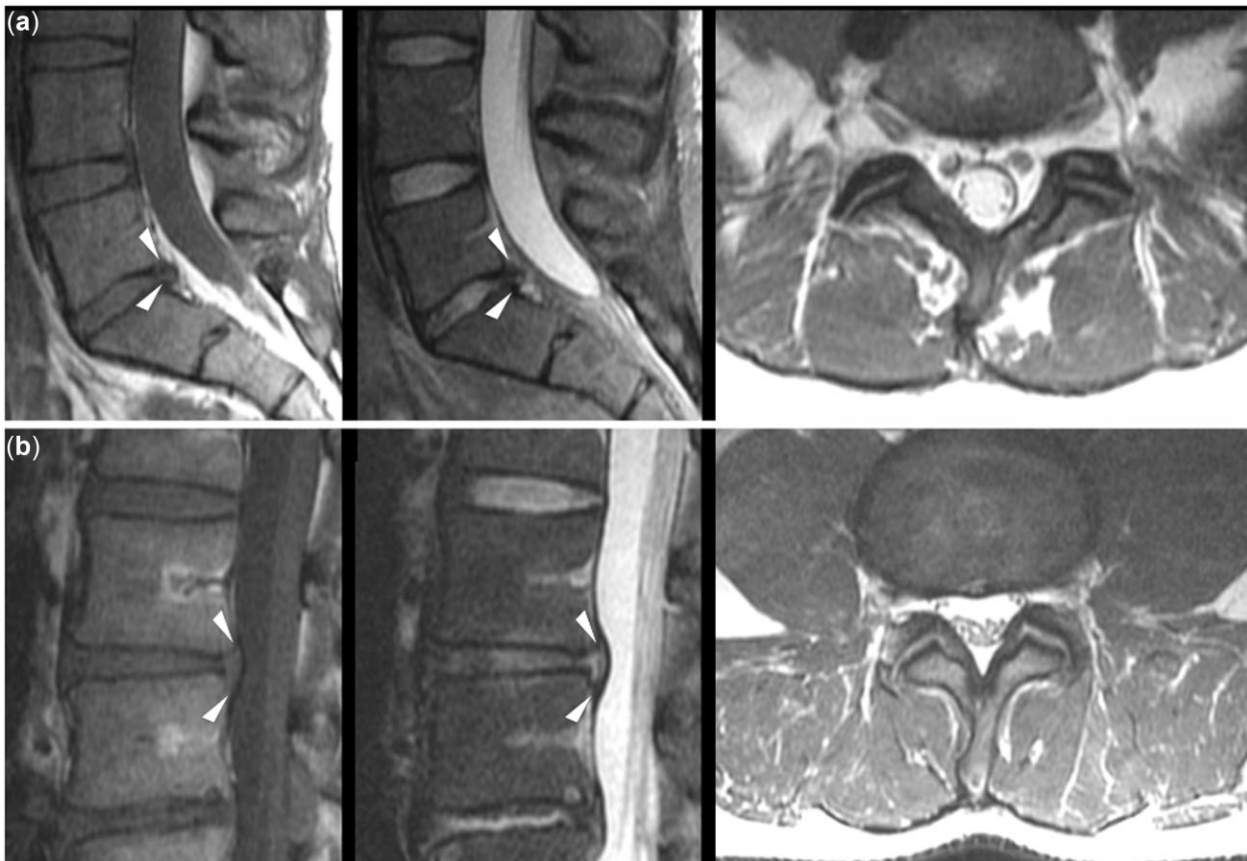


Figure 4. Disc herniation. Example cases for disc protrusion (a; arrowheads) and disc extrusion (b; arrowheads) on sagittal T1- and T2-weighted sequences and axial T2-weighted sequences. A disc protrusion is considered in case of a focal herniation of disc material beyond the margins of the adjacent vertebral bodies, while a disc extrusion is a focal herniation of disc nuclear material through an annular defect. In both presented cases, absent to minor resulting constriction of the thecal sac is shown on axial sequences.

Table 6. Facet and sacroiliac joint changes

| | 0 | 1 | 2 | 3 | Sequences |
|---|-----------|---|---|--|---|
| Facet joint (FJ) | | | | | |
| Joint Space | None | Narrowing, small osteophytes or hypertrophy | Narrowing, moderate osteophytes or hypertrophy | Narrowing, large osteophytes or severe hypertrophy | SAG T2 FS AX T2 AX T1 AX T2 FS |
| Joint Fluid | Absent | Present | | | |
| Sacroiliac joint (SIJ) | | | | | |
| Appearance | Normal | Abnormal | | | SAG T2 FS COR T1 |
| Joint Space | Normal | Degenerative | Erosions | | COR T1 |
| Bone Marrow | Normal | Edema | Fatty transformation | | SAG T1 COR T1 |
| Bone | Normal | Insufficiency fractures | Osteitis condensans ilii | Other | SAG T1 COR T1 |
| Lumbosacral Transitional Vertebrae Type | None | Large transverse processes (>2.1 cm) | Large transverse process articulating with the sacrum | Large transverse process fused with sacrum | SAG T1 SAG T2 FS COR T1 |
| Lumbosacral Transitional Vertebrae Location | Bilateral | Left | Right | Asymmetric | SAG T1 SAG T2 FS COR T1 |

This table illustrates the scoring scheme for changes of the facet joints (FJs) and sacroiliac joints (SIJs) and the sequences used for evaluation of different categories. In addition, presence and degree of lumbosacral transitional vertebrae (LSTV) should be assessed.

transitional vertebrae (LSTV) are evaluated based on a rating scheme modified from that of Castellvi et al. (Table 6) [58, 59]. The inter-rater reliability was demonstrated to be excellent for the detection ($\kappa = 0.93$) and classification ($\kappa = 0.83$) of LSTV based on MRI [60].

Stenosis

Evaluation of central canal stenosis is made according to the contour of the thecal sac and amount of cerebrospinal fluid (CSF) space around the spinal cord. In detail, discrimination is made between no thecal sac constriction, mild constriction

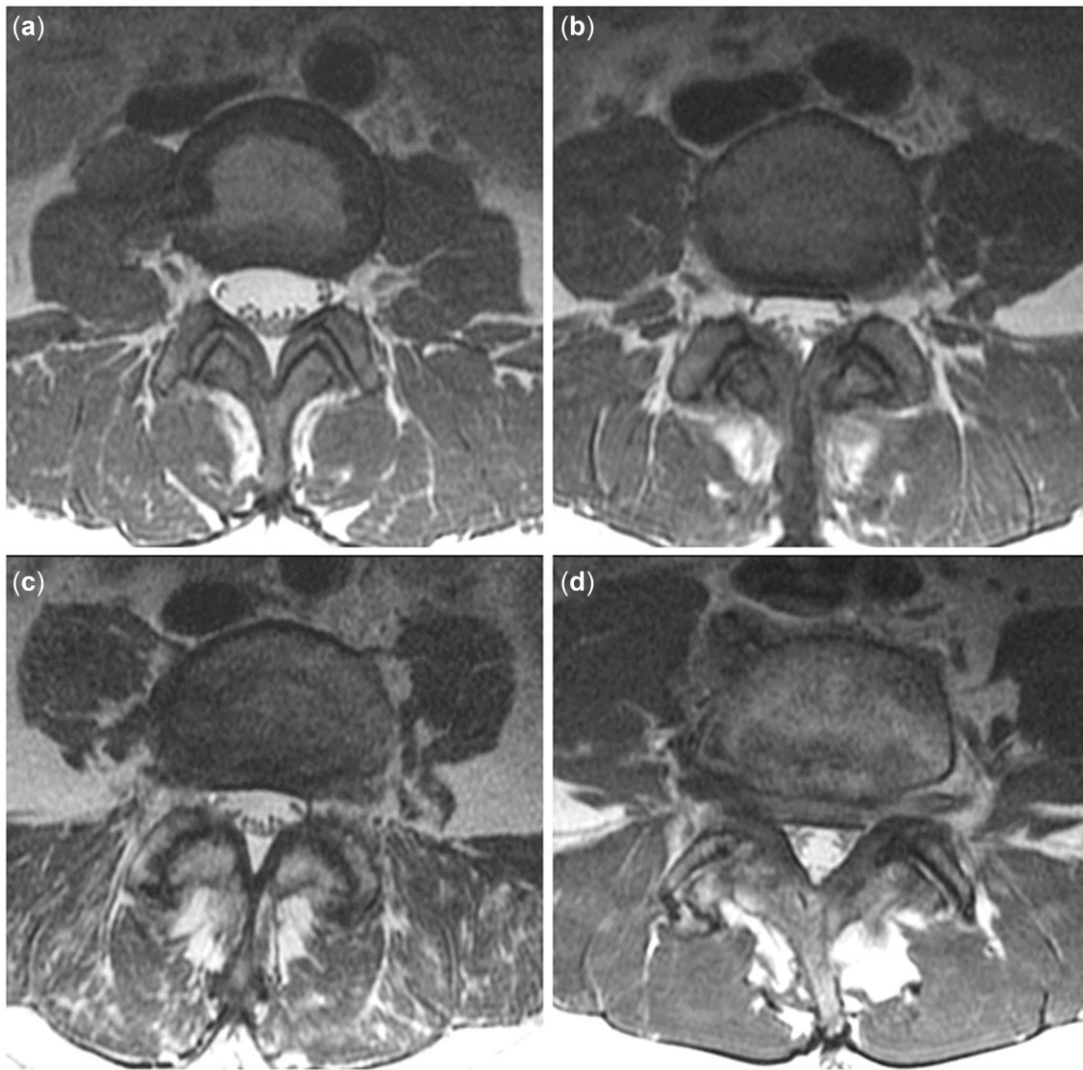


Figure 5. Facet joint (FJ) degenerative changes. Examples for grading of FJ changes: normal appearance (a); narrowing, small osteophytes or hypertrophy (b); narrowing, moderate osteophytes or hypertrophy (c); and narrowing, large osteophytes or severe hypertrophy (d).

(minimal loss of CSF around rootlets), moderate grade (CSF diminished but present), and severe grade of central canal stenosis with complete loss of CSF signal (Table 7). In addition, features indicative of congenital narrowing of the spinal canal (i.e., shorter pedicular length and related smaller cross-sectional spinal canal area) are documented (Table 7) [61]. Example cases for spinal canal narrowing are given by Figure 6.

With regard to the course of the exiting spinal nerve roots, contact to surrounding compressive structures (e.g., herniated intervertebral discs or FJ arthropathy) with or without deviation and side are evaluated for the subarticular zone. For the neuroforamina, stenosis is classified as mild (i.e., slight deformity of epidural fat, still completely surrounding nerve root), moderate (i.e., marked deformity of epidural fat, only partially surrounding nerve root), and severe (i.e., obliteration of epidural fat), according to changes in epidural fat configuration as a surrogate of compression at the level of the neuroforamina (Table 7) [62]. Inter-rater agreement for the grading of neuroforaminal stenosis has been reported to be excellent ($\kappa > 0.90$), with slightly lower agreement for intra-rater comparisons ($\kappa > 0.79$) [62].

Discussion

Within the BACPAC Research Program, MRI studies are being used to facilitate better understanding of pain mechanisms in chronic LBP by developing, establishing, and translating standardized MRI-based methods. A main goal is to identify specific phenotypes of LBP that would enable reliable guidance for patient selection for certain treatment regimens and to predict responses to treatments, with the ultimate goal to improve clinical management and therapy.

The SOPs we have described address two sources of variability in MRI for patients with LBP—image acquisition and image interpretation. While lumbar MRI can be a powerful modality for LBP assessment in cases where imaging is warranted, imaging protocols and MRI systems vary greatly between sites. Imaging within the BACPAC Research Program implements a standardized procedure for scanning, whilst technical variations and particularities between scanners at different sites are acknowledged by recommending ranges for pulse sequence protocols. The herein presented SOPs may help to better integrate data across studies and sites to facilitate robust analyses and inferences using much larger datasets than would otherwise be available. Furthermore,

Table 7. Stenosis

| | 0 | 1 | 2 | 3 | Sequences |
|--|----------------------------|--|--|-------------------------------------|---------------------|
| Central Canal | No thecal sac constriction | Mild constriction, minimal loss of CSF around rootlets | CSF diminished but present | Complete loss of CSF | SAG T2 FS AX T2 |
| Congenital Narrowing of Central Canal | No | Yes | | | SAG T2 FS AX T2 |
| Subarticular Zone Stenosis Characteristics | No nerve root contact | Nerve root contact without deviation | Nerve root compression | | SAG T2 FS AX T2 |
| Subarticular Zone Stenosis Side | Left | Right | Bilateral | | SAG T2 FS AX T2 |
| Neuroforaminal Stenosis Characteristics | Normal epidural fat | Mild—slight deformity of epidural fat, still completely surrounding the nerve root | Moderate—marked deformity of epidural fat, only partially surrounding nerve root | Severe—obliteration of epidural fat | SAG T1 SAG T2 FS |
| Neuroforaminal Stenosis Side | Left | Right | Bilateral | | SAG T1 SAG T2 FS |

This table outlines the scoring scheme for central canal stenosis and neuroforaminal stenosis or stenosis at the subarticular zone and the sequences used for evaluation of such stenotic changes.

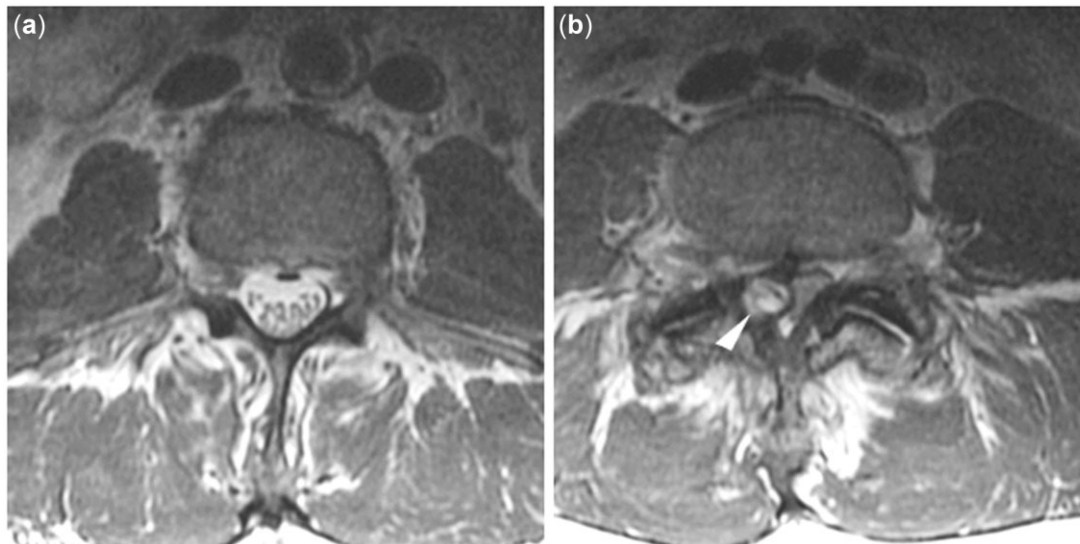


Figure 6. Spinal canal stenosis. Normal configuration and diameter of the spinal canal (a) and severely narrowed spinal canal with complete loss of cerebrospinal fluid (CSF) signal due to degenerative changes with a synovial cyst (b; arrowhead).

evaluation of better harmonized MRI data of the lumbar spine across studies and sites within and outside of BACPAC studies is supported by these SOPs, given that variability in used equipment and pulse sequence protocols could be reduced. For evaluation of conventional MRI using T1- and T2-weighted sequences in LBP, structured reporting is established to reduce inconsistent reporting or subjective misinterpretations of findings during image reading. Structured reporting uses predefined terms and formats to generate a radiological report, thus ensuring a high degree of standardized and organized information that is presented in template context [63, 64]. Structured reporting is not broadly utilized in LBP, but it may help to reduce variations during image reading, and it could thus provide condensed information relevant for structural alterations potentially linked to pain perception and for identification of imaging-based biomarkers.

Potential biomarkers of LBP that are commonly detected on routine clinical scans include BM lesions at the vertebral endplates, disc bulges and herniation, and spondylolysis [10–12]. The proposed comprehensive scoring system is based on visual reading of T1- and T2-weighted sequences with structured reporting. A strength is that this scoring system integrates previously established grading schemes within a standardized approach. The majority of such schemes has demonstrated at least substantial inter- and/or intra-rater reliability (e.g., classification of Modic-type endplate changes or Pfirrmann grading for degenerative disc disease) [27, 28, 45–48]. On the other hand, potential weaknesses include the qualitative/semi-quantitative nature of analyses by visual image reading and bias towards only structural findings rather than compositional findings. Related to this, the relationships between pathologies evaluated by these established grading schemes and pain might be variable, and thus, the

clinical implications are unclear. For instance, it has been reported that Modic-type endplate changes have inconsistent associations with pain [12, 65–70]. Inconsistencies may stem from several sources, including imprecise description of Modic-type endplate changes for clinical reports, utilization of MRI equipment that introduces grading bias, or acquisition of imaging sequences that inadvertently misrepresent these changes [71]. Specifically, omission of basic methodological details and, most notably, restriction to mainly qualitative/semi-quantitative, non-standardized evaluation of MRI data for Modic-type endplate changes make it difficult to draw more final conclusions about the correlation of LBP and vertebral endplate pathology [71].

Several novel MRI-based methods are undergoing research and development that may allow detection of biomarkers not seen on conventional lumbar MRI on the way to improved understanding of LBP mechanisms. For example, magnetic resonance spectroscopy (MRS) was used to quantify spectral features related to intervertebral disc structure and acidity, and results from MRS correlated well with provocative discography, thus could potentially support improved surgical outcomes among patients with chronic LBP [72]. Furthermore, ultra-short echo-time (UTE) imaging and chemical shift encoding-based water-fat MRI (CSE-MRI) have been proposed to be more sensitive to endplate damage or BM pathology and allow both to be quantified, yet without the need for specialized MRI hardware or application of contrast agents [73–79]. Structural damage of the endplate is believed to trigger endplate neo-innervation and painful endplate BM lesions, and cartilage endplate fibrosis blocks nutrient transport to the disc cells, thereby hindering cell survival, disc matrix homeostasis, and regenerative potential [80, 81].

Another novel MRI-based approach that may provide important information related to LBP is CSE-MRI for assessment of paraspinal muscle quality, which may not be well characterized on routine MRI. This approach permits spatial measurements of fat fraction within the paraspinal muscles (e.g., erector spinae or multifidus muscles) [82–87]. Paraspinal muscle fat fractions showed significant correlations to isometric muscle strength as well as vertebral BM fat fractions, hence potentially reflecting the actual (patho)physiological muscle status [82, 87]. Furthermore, in a study investigating the interplay between vertebral endplate pathology and paraspinal muscle quality in patients with chronic LBP, cartilage endplate defects at the lower lumbar spine were predictive of pain when adjacent to paraspinal musculature with increased fat fractions [73]. Yet the distinct role of paraspinal musculature and particularly the fat fraction as a quantitative parameter remain largely unclear to date in patients with LBP.

While the efforts of the BACPAC Spine Imaging Working Group focus on the spine with distinct SOPs for spinal MRI protocols, it has to be acknowledged that particularly in patients suffering from chronic LBP, perceived pain may not only relate to the level of the spine. Thus, novel conceptualizations and mechanistic descriptors that involve interactions and structures beyond the lumbar spine might play an important role as well. Specifically, besides nociceptive pain (arising from ongoing input from tissue injury) and neuropathic pain (arising from injury to the peripheral or central nervous system), the concept of nociplastic pain has been described for chronic pain states that are not related to obvious nociceptor activation or neuropathy, whereas clinical and psychophysical findings suggest alterations

in nociceptive function [88, 89]. As such, nociplastic pain can stem from altered pain-related sensory pathways that relate to enhanced sensitivity, and thus nociplastic pain may exist either as a comorbid or isolated state in patients with chronic pain that has been predominantly characterized as nociceptive or neuropathic [16, 88]. Particularly patients suffering from non-specific chronic LBP may show a continuum of nociceptive, neuropathic, and nociplastic components, with related increased activation of brain regions that contribute to the processing of pain and other sensory functions [88, 90–92]. Concerning patients with such mixed pain, lumbar MRI may contribute to the detection of the site that initiated pain, but imaging of central mechanisms (e.g., by functional MRI of the brain) might be needed to provide a more complete picture of the complex individual pain states.

Another relevant aspect beyond the lumbar spine might be the analysis of whole-body composition in relation to sarcopenia, which is defined as a progressive and generalized skeletal muscle disorder that involves the accelerated loss of muscle mass and function [93, 94]. While paraspinal muscle structure is routinely captured by standard lumbar MRI exams at least for some spinal levels, it is often neglected during reporting among patients with LBP, and investigations of dedicated muscle composition beyond the musculature adjacent to the spinal column are uncommon for LBP. However, it has been suggested that sarcopenia is correlated with back muscle strength and in turn also with the presence of degenerative spinal disorders [95–97]. With improved MRI hardware and software technology, it becomes possible to acquire high-quality images of large parts of the whole body in reasonable amounts of time, thus potentially making assessments of body and muscle composition beyond the direct paraspinal compartments also attractive for research in the field of chronic LBP.

Conclusion

Management of patients suffering from LBP is challenging and requires development of diagnostic techniques to identify specific patient subgroups and phenotypes in order to customize treatment and predict clinical outcome. While lumbar MRI is frequently performed in patients with LBP, it has not yet developed into a reliable and standardized tool for these purposes. The BACPAC Spine Imaging Working Group has developed SOPs that will facilitate identification of biomarkers in lumbar MRI, which will help to support patient selection for certain treatment regimens and to predict responses to treatment. Moreover, the approach and methods outlined in this article may also serve as a recommendation for other centers performing MRI acquisitions in patients with LBP, thus potentially supporting standardization of clinical routine MRI acquisitions and reporting. Ultimately, the SOPs presented may facilitate the integration of better harmonized MRI data of the lumbar spine across studies and sites within and outside of BACPAC studies.

Funding

This research was supported by the National Institutes of Health through the Helping to End Addiction Long-termSM Initiative, or NIH Heal Initiative, as well as by the German Academic Exchange Service (Deutscher Akademischer Austauschdienst, DAAD: N.S.), the Joachim

Herz Foundation (N.S.), and the Rolf W. Günther Foundation (N.S.). L.N. is principal investigator of service agreement with United Healthcare.

Conflicts of interest: There are no conflicts of interest to report.

Supplement sponsorship

This article appears as part of the supplement entitled “Back Pain Consortium (BACPAC) Research Program” supported by the National Institutes of Health through the NIH HEAL Initiative under award number AR076730-01.

Disclaimer

The content is solely the responsibility of the authors and does not necessarily represent the official views of the National Institutes of Health or its NIH HEAL Initiative.

Abbreviations

| | |
|---------|---|
| 3D | Three-dimensional |
| BACPAC | Back Pain Consortium |
| BM | Bone marrow |
| CSE-MRI | Chemical shift encoding-based water-fat MRI |
| CSF | Cerebrospinal fluid |
| FJ | Facet joint |
| FOV | Field of view |
| FS | Fat suppression |
| FSE | Fast spin-echo |
| LBP | Low back pain |
| LSTV | Lumbosacral transitional vertebrae |
| MRI | Magnetic resonance imaging |
| MRN | Magnetic resonance neurography |
| MRS | Magnetic resonance spectroscopy |
| NEX | Number of excitations |
| SIJ | Sacroiliac joint |
| SOP | Standard operating procedure |
| TE | Echo time |
| TR | Repetition time |
| UTE | Ultra-short echo-time |

References

- Sheehan NJ. Magnetic resonance imaging for low back pain: Indications and limitations. *Postgrad Med J* 2010;86(1016):374–8.
- Chou D, Samartzis D, Bellabarba C, et al. Degenerative magnetic resonance imaging changes in patients with chronic low back pain: A systematic review. *Spine* 2011;36(21 Suppl):S43–53.
- Wassenaar M, van Rijn RM, van Tulder MW, et al. Magnetic resonance imaging for diagnosing lumbar spinal pathology in adult patients with low back pain or sciatica: A diagnostic systematic review. *Eur Spine J* 2012;21(2):220–7.
- Roudsari B, Jarvik JG. Lumbar spine MRI for low back pain: Indications and yield. *AJR Am J Roentgenol* 2010;195(3):550–9.
- Sollmann N, Monch S, Riederer I, Zimmer C, Baum T, Kirschke JS. Imaging of the degenerative spine using a sagittal T2-weighted DIXON turbo spin-echo sequence. *Eur J Radiol* 2020;131:109204.
- Chou R, Qaseem A, Owens DK, Shekelle P, Clinical Guidelines Committee of the American College of Physicians. Diagnostic imaging for low back pain: Advice for high-value health care from the American College of Physicians. *Ann Intern Med* 2011;154(3):181–9.
- Maher C, Underwood M, Buchbinder R. Non-specific low back pain. *Lancet* 2017;389(10070):736–47.
- Koes BW, van Tulder MW, Thomas S. Diagnosis and treatment of low back pain. *BMJ* 2006;332(7555):1430–4.
- Brinjikji W, Luetmer PH, Comstock B, et al. Systematic literature review of imaging features of spinal degeneration in asymptomatic populations. *AJNR Am J Neuroradiol* 2015;36(4):811–6.
- Hartvigsen J, Hancock MJ, Kongsted A, et al.; Lancet Low Back Pain Series Working Group. What low back pain is and why we need to pay attention. *Lancet* 2018;391(10137):2356–67.
- Panagopoulos J, Magnussen JS, Hush J, et al. Prospective comparison of changes in lumbar spine MRI findings over time between individuals with acute low back pain and controls: An exploratory study. *AJNR Am J Neuroradiol* 2017;38(9):1826–32.
- Brinjikji W, Diehn FE, Jarvik JG, et al. MRI findings of disc degeneration are more prevalent in adults with low back pain than in asymptomatic controls: A systematic review and meta-analysis. *AJNR Am J Neuroradiol* 2015;36(12):2394–9.
- Latremoliere A, Woolf CJ. Central sensitization: A generator of pain hypersensitivity by central neural plasticity. *J Pain* 2009;10(9):895–926.
- Sanzarelli I, Merlini L, Rosa MA, et al. Central sensitization in chronic low back pain: A narrative review. *J Back Musculoskelet Rehabil* 2016;29(4):625–33.
- Roussel NA, Nijs J, Meeus M, Mylius V, Fayt C, Oostendorp R. Central sensitization and altered central pain processing in chronic low back pain: Fact or myth? *Clin J Pain* 2013;29(7):625–38.
- Woolf CJ. Central sensitization: Implications for the diagnosis and treatment of pain. *Pain* 2011;152(Suppl 3):S2–S15.
- Sollmann N, Weidlich D, Cervantes B, Klupp E, et al. T2 mapping of lumbosacral nerves in patients suffering from unilateral radicular pain due to degenerative disc disease. *J Neurosurg Spine* 2019;1–9 (doi: 10.3171/2018.10.SPINE181172).
- Dessouky R, Khaleel M, Khalifa DN, Tantawy HI, Chhabra A. Magnetic Resonance Neurography of the Lumbosacral Plexus in Failed Back Surgery Syndrome. *Spine* 2018;43(12):839–47.
- Chhabra A, Belzberg AJ, Rosson GD, et al. Impact of high resolution 3 tesla MR neurography (MRN) on diagnostic thinking and therapeutic patient management. *European Radiology* 2016;26(5):1235–44.
- Chhabra A, Rozen S, Scott K. Three-dimensional MR neurography of the lumbosacral plexus. *Semin Musculoskelet Radiol* 2015;19(2):149–59.
- Cho Sims G, Boothe E, Joodi R, Chhabra A. 3D MR neurography of the lumbosacral plexus: Obtaining optimal images for selective longitudinal nerve depiction. *AJNR Am J Neuroradiol* 2016;37(11):2158–62.
- Soldatos T, Andreisek G, Thawait GK, et al. High-resolution 3-T MR neurography of the lumbosacral plexus. *Radiographics* 2013;33(4):967–87.
- Modic MT, Steinberg PM, Ross JS, Masaryk TJ, Carter JR. Degenerative disk disease: Assessment of changes in vertebral body marrow with MR imaging. *Radiology* 1988;166(1 Pt 1):193–9.
- Rahme R, Moussa R. The modic vertebral endplate and marrow changes: Pathologic significance and relation to low back pain and segmental instability of the lumbar spine. *AJNR Am J Neuroradiol* 2008;29(5):838–42.
- Dudli S, Fields AJ, Samartzis D, Karppinen J, Lotz JC. Pathobiology of Modic changes. *Eur Spine J* 2016;25(11):3723–34.
- de Roos A, Kressel H, Spritzer C, Dalinka M. MR imaging of marrow changes adjacent to end plates in degenerative lumbar disk disease. *AJR Am J Roentgenol* 1987;149(3):531–4.
- Wang Y, Videman T, Niemelainen R, Battie MC. Quantitative measures of modic changes in lumbar spine magnetic resonance imaging: Intra- and inter-rater reliability. *Spine* 2011;36(15):1236–43.
- Jones A, Clarke A, Freeman BJ, Lam KS, Grevitt MP. The Modic classification: Inter- and intraobserver error in clinical practice. *Spine* 2005;30(16):1867–9.

29. Braithwaite I, White J, Saifuddin A, Renton P, Taylor BA. Vertebral end-plate (Modic) changes on lumbar spine MRI: Correlation with pain reproduction at lumbar discography. *Eur Spine J* 1998;7(5):363–8.
30. Ito M, Incorvaia KM, Yu SF, Fredrickson BE, Yuan HA, Rosenbaum AE. Predictive signs of discogenic lumbar pain on magnetic resonance imaging with discography correlation. *Spine* 1998; 23(11):1252–8. discussion 59–60.
31. O'Neill C, Kurgansky M, Kaiser J, Lau W. Accuracy of MRI for diagnosis of discogenic pain. *Pain Physician* 2008;11 (3):311–26.
32. Thompson KJ, Dagher AP, Eckel TS, Clark M, Reinig JW. Modic changes on MR images as studied with provocative diskography: Clinical relevance—a retrospective study of 2457 disks. *Radiology* 2009;250(3):849–55.
33. Weishaupt D, Zanetti M, Hodler J, et al. Painful lumbar disk derangement: Relevance of endplate abnormalities at MR imaging. *Radiology* 2001;218(2):420–7.
34. Jevtic V. Magnetic resonance imaging appearances of different disc-vertebral lesions. *Eur Radiol* 2001;11(7):1123–35.
35. Blumenthal SL, Roach J, Herring JA. Lumbar Scheuermann's. A clinical series and classification. *Spine* 1987;12(9):929–32.
36. Sardar ZM, Ames RJ, Lenke L. Scheuermann's Kyphosis: Diagnosis, management, and selecting fusion levels. *J Am Acad Orthop Surg* 2019;27(10):e462–72.
37. Ziegler R, Scheidt-Nave C, Leidig-Bruckner G. What is a vertebral fracture? *Bone* 1996;18(Suppl 3):169S–77S.
38. Genant HK, Wu CY, van Kijik C, Nevitt MC. Vertebral fracture assessment using a semiquantitative technique. *J Bone Miner Res* 1993;8(9):1137–48.
39. Compston JE, McClung MR, Leslie WD. Osteoporosis. *Lancet* 2019;393(10169):364–76.
40. Loffler MT, Sollmann N, Mei K, et al. X-ray-based quantitative osteoporosis imaging at the spine. *Osteoporos Int* 2020;31 (2):233–50.
41. Sollmann N, Loffler MT, Kronthaler S, et al. MRI-based quantitative osteoporosis imaging at the spine and femur. *J Magn Reson Imaging* 2021;54(1):12–35.
42. Link TM, Kazakia G. Update on imaging-based measurement of bone mineral density and quality. *Curr Rheumatol Rep* 2020;22(5):13.
43. Schousboe JT. Epidemiology of vertebral fractures. *J Clin Densitom* 2016;19(1):8–22.
44. Sollmann N, Kirschke JS, Kronthaler S, et al. Imaging of the osteoporotic spine: Quantitative approaches in diagnostics and for the prediction of the individual fracture risk. *Rofo* 2022; (doi: 10.1055/a-1770-4626).
45. Pfirrmann CW, Metzdorf A, Zanetti M, Hodler J, Boos N. Magnetic resonance classification of lumbar intervertebral disc degeneration. *Spine* 2001;26(17):1873–8.
46. Carrino JA, Lurie JD, Tosteson AN, et al. Lumbar spine: Reliability of MR imaging findings. *Radiology* 2009;250(1):161–70.
47. Urrutia J, Besa P, Campos M, et al. The Pfirrmann classification of lumbar intervertebral disc degeneration: An independent inter- and intra-observer agreement assessment. *Eur Spine J* 2016;25 (9):2728–33.
48. Yu LP, Qian WW, Yin GY, Ren YX, Hu ZY. MRI assessment of lumbar intervertebral disc degeneration with lumbar degenerative disease using the Pfirrmann grading systems. *PLoS One* 2012;7 (12):e48074.
49. Pfirrmann CW, Dora C, Schmid MR, Zanetti M, Hodler J, Boos N. MR image-based grading of lumbar nerve root compromise due to disk herniation: Reliability study with surgical correlation. *Radiology* 2004;230(2):583–8.
50. Fardon DF, Williams AL, Dohring EJ, Murtagh FR, Gabriel Rothman SL, Sze GK. Lumbar disc nomenclature: Version 2.0: Recommendations of the combined task forces of the North American Spine Society, the American Society of Spine Radiology and the American Society of Neuroradiology. *Spine J* 2014;14 (11):2525–45.
51. Fardon DF, Milette PC, Combined Task Forces of the North American Spine Society, American Society of Spine Radiology, and American Society of Neuroradiology. Nomenclature and classification of lumbar disc pathology. Recommendations of the combined task forces of the North American Spine Society, American Society of Spine Radiology, and American Society of Neuroradiology. *Spine* 2001;26(5):E93–113.
52. Pathria M, Sartoris DJ, Resnick D. Osteoarthritis of the facet joints: Accuracy of oblique radiographic assessment. *Radiology* 1987;164 (1):227–30.
53. Fujiwara A, Tamai K, Yamato M, et al. The relationship between facet joint osteoarthritis and disc degeneration of the lumbar spine: An MRI study. *Eur Spine J* 1999;8(5):396–401.
54. Weishaupt D, Zanetti M, Boos N, Hodler J. MR imaging and CT in osteoarthritis of the lumbar facet joints. *Skeletal Radiol* 1999;28 (4):215–9.
55. Poddubnyy D, Weineck H, Diekhoff T, et al. Clinical and imaging characteristics of osteitis condensans ilii as compared with axial spondyloarthritis. *Rheumatology (Oxford)* 2020;59(12):3798–806.
56. Clarke DP, Higgins JN, Valentine AR, Black C. Magnetic resonance imaging of osteitis condensans ilii. *Br J Rheumatol* 1994;33 (6):599–600.
57. Mandl P, Navarro-Compan V, Terslev L, et al.; European League Against Rheumatism (EULAR). EULAR recommendations for the use of imaging in the diagnosis and management of spondyloarthritis in clinical practice. *Ann Rheum Dis* 2015;74(7):1327–39.
58. Castellvi AE, Goldstein LA, Chan DP. Lumbosacral transitional vertebrae and their relationship with lumbar extradural defects. *Spine* 1984;9(5):493–5.
59. Nardo L, Alizai H, Virayavanich W, et al. Lumbosacral transitional vertebrae: Association with low back pain. *Radiology* 2012;265 (2):497–503.
60. Farshad-Amacker NA, Lurie B, Herzog RJ, Farshad M. Interreader and intermodality reliability of standard anteroposterior radiograph and magnetic resonance imaging in detection and classification of lumbosacral transitional vertebra. *Spine J* 2014;14(8):1470–5.
61. Singh K, Samartzis D, Vaccaro AR, et al. Congenital lumbar spinal stenosis: A prospective, control-matched, cohort radiographic analysis. *Spine J* 2005;5(6):615–22.
62. Lee S, Lee JW, Yeom JS, Kim KJ, et al. A practical MRI grading system for lumbar foraminal stenosis. *AJR American Journal of Roentgenology* 2010;194(4):1095–8.
63. Liu D, Zucherman M, Tulloss WB Jr. Six characteristics of effective structured reporting and the inevitable integration with speech recognition. *J Digit Imaging* 2006;19(1):98–104.
64. Kahn CE Jr, Langlotz CP, Burnside ES, et al. Toward best practices in radiology reporting. *Radiology* 2009;252(3):852–6.
65. Jensen TS, Karppinen J, Sorensen JS, Niinimäki J, Leboeuf-Yde C. Vertebral endplate signal changes (Modic change): A systematic literature review of prevalence and association with non-specific low back pain. *Eur Spine J* 2008;17(11):1407–22.
66. Zhang YH, Zhao CQ, Jiang LS, Chen XD, Dai LY. Modic changes: A systematic review of the literature. *Eur Spine J* 2008;17 (10):1289–99.
67. Albert HB, Kjaer P, Jensen TS, Sorensen JS, Bendix T, Manniche C. Modic changes, possible causes and relation to low back pain. *Med Hypotheses* 2008;70(2):361–8.
68. Herlin C, Kjaer P, Espeland A, et al. Modic changes, their associations with low back pain and activity limitation: A systematic literature review and meta-analysis. *PLoS One* 2018;13(8):e0200677.
69. Laustsen AF, Bech-Azeddine R. Do Modic changes have an impact on clinical outcome in lumbar spine surgery? A systematic literature review. *Eur Spine J* 2016;25(11):3735–45.
70. Lawan A, Crites Videman J, Battie MC. The association between vertebral endplate structural defects and back pain: A systematic review and meta-analysis. *Eur Spine J* 2021;30(9):2531–48.
71. Fields AJ, Battie MC, Herzog RJ, et al.; ISSLS Degenerative Spinal Phenotypes Group. Measuring and reporting of vertebral endplate bone marrow lesions as seen on MRI (Modic changes):

- Recommendations from the ISSLS Degenerative Spinal Phenotypes Group. *Eur Spine J* 2019;28(10):2266–74.
72. Gornet MG, Peacock J, Claude J, et al. Magnetic resonance spectroscopy (MRS) can identify painful lumbar discs and may facilitate improved clinical outcomes of lumbar surgeries for discogenic pain. *Eur Spine J* 2019;28(4):674–87.
 73. Bailey JF, Fields AJ, Ballatori A, et al. The relationship between endplate pathology and patient-reported symptoms for chronic low back pain depends on lumbar paraspinal muscle quality. *Spine* 2019;44(14):1010–7.
 74. Krug R, Joseph GB, Han M, et al. Associations between vertebral body fat fraction and intervertebral disc biochemical composition as assessed by quantitative MRI. *J Magn Reson Imaging* 2019;50(4):1219–26.
 75. Fields AJ, Han M, Krug R, Lotz JC. Cartilaginous end plates: Quantitative MR imaging with very short echo times-orientation dependence and correlation with biochemical composition. *Radiology* 2015;274(2):482–9.
 76. Berg-Johansen B, Han M, Fields AJ, et al. Cartilage endplate thickness variation measured by ultrashort echo-time MRI is associated with adjacent disc degeneration. *Spine* 2018;43(10):E592–600.
 77. Fields AJ, Ballatori A, Han M, et al. Measurement of vertebral endplate bone marrow lesion (Modic change) composition with water-fat MRI and relationship to patient-reported outcome measures. *Eur Spine J* 2021;30(9):2549–56.
 78. Wang L, Han M, Wong J, et al. Evaluation of human cartilage endplate composition using MRI: Spatial variation, association with adjacent disc degeneration, and in vivo repeatability. *J Orthop Res* 2021;39(7):1470–8.
 79. Bonnheim NB, Wang L, Lazar AA, et al. The contributions of cartilage endplate composition and vertebral bone marrow fat to intervertebral disc degeneration in patients with chronic low back pain. *Eur Spine J* 2022;31(7):1866–72.
 80. Fields AJ, Liebenberg EC, Lotz JC. Innervation of pathologies in the lumbar vertebral end plate and intervertebral disc. *Spine J* 2014;14(3):513–21.
 81. Wong J, Sampson SL, Bell-Briones H, et al. Nutrient supply and nucleus pulposus cell function: Effects of the transport properties of the cartilage endplate and potential implications for intradiscal biologic therapy. *Osteoarthritis Cartilage* 2019;27(6):956–64.
 82. Sollmann N, Dieckmeyer M, Schlaeger S, et al. Associations between lumbar vertebral bone marrow and paraspinal muscle fat compositions-an investigation by chemical shift encoding-based water-fat MRI. *Front Endocrinol (Lausanne)* 2018;9:563.
 83. Dieckmeyer M, Inhuber S, Schlaeger S, et al. Texture features of proton density fat fraction maps from chemical shift encoding-based MRI predict paraspinal muscle strength. *Diagnostics (Basel)* 2021;11(2):239.
 84. Burian E, Syvari J, Dieckmeyer M, et al. Age- and BMI-related variations of fat distribution in sacral and lumbar bone marrow and their association with local muscle fat content. *Sci Rep* 2020;10(1):9686.
 85. Burian E, Becherucci EA, Junker D, et al. Association of cervical and lumbar paraspinal muscle composition using texture analysis of MR-based proton density fat fraction maps. *Diagnostics (Basel)* 2021;11(10):1929.
 86. Sollmann N, Bonnheim NB, Joseph GB, Chachad R, et al. Paraspinal muscle in chronic low back pain: Comparison between standard parameters and chemical shift encoding-based water-fat MRI. *J Magn Reson Imaging* 2022; (doi: 10.1002/jmri.28145).
 87. Schlaeger S, Inhuber S, Rohrmeier A, et al. Association of paraspinal muscle water-fat MRI-based measurements with isometric strength measurements. *Eur Radiol* 2019;29(2):599–608.
 88. Fitzcharles M-A, Cohen SP, Clauw DJ, Littlejohn G, Usui C, Häuser W. Nociceptive pain: Towards an understanding of prevalent pain conditions. *Lancet* 2021;397(10289):2098–110.
 89. Kosek E, Cohen M, Baron R, et al. Do we need a third mechanistic descriptor for chronic pain states? *Pain* 2016;157(7):1382–6.
 90. Freynhagen R, Rolke R, Baron R, et al. Pseudoradicular and radicular low-back pain—a disease continuum rather than different entities? Answers from quantitative sensory testing. *Pain* 2008;135(1–2):65–74.
 91. Forster M, Mahn F, Gockel U, et al. Axial low back pain: One painful area—many perceptions and mechanisms. *PLoS One* 2013;8(7):e68273.
 92. Giesecke T, Gracely RH, Grant MA, et al. Evidence of augmented central pain processing in idiopathic chronic low back pain. *Arthritis Rheum* 2004;50(2):613–23.
 93. Cruz-Jentoft AJ, Bahat G, Bauer J, et al.; Writing Group for the European Working Group on Sarcopenia in Older P, the Extended Group for EWGSOP2. Sarcopenia: Revised European consensus on definition and diagnosis. *Age Ageing* 2019;48(1):16–31.
 94. Cruz-Jentoft AJ, Sayer AA. Sarcopenia. *Lancet* 2019;393(10191):2636–46.
 95. Toyoda H, Hoshino M, Ohya S, et al. The association of back muscle strength and sarcopenia-related parameters in the patients with spinal disorders. *Eur Spine J* 2019;28(2):241–9.
 96. Eguchi Y, Suzuki M, Yamanaka H, et al. Associations between sarcopenia and degenerative lumbar scoliosis in older women. *Scoliosis Spinal Disord* 2017;12(1):9.
 97. Park S, Kim HJ, Ko BG, et al. The prevalence and impact of sarcopenia on degenerative lumbar spinal stenosis. *Bone Joint J* 2016; 98-B(8):1093–8.